Surface Chemistry

Strain-Induced Formation of Subsurface Species in Transition Metals**

*Jeff Greeley, William P. Krekelberg, and Manos Mavrikakis**

Surface strain has recently been shown to have a significant effect on the reactivity of transition-metal surfaces,[1] and numerous examples of strain effects on both the thermochemistry and kinetics of surface reactions have been identified.[2–7] Several of these studies focused on strain induced by epitaxial metal overlayers, but recently it has been demonstrated that strain from another source, namely, dislocations that intersect crystal surfaces, likewise causes significant changes in surface reactivity.[8] This suggests that a careful study on the effect of strain on catalytic processes might yield substantial insights into the effect of defects on these processes. Defects, in turn, have been shown to dominate the reactivity of certain surface reactions.[9] In particular, an analysis of the manner in which strain influences the population of subsurface species in transition metals could contribute to an understanding of the more general problem of how dislocation-induced surface defects mediate the transfer of adsorbates to subsurface regions. Such an analysis could permit a comparison between the behavior of subsurface species on single-crystal and polycrystalline metals,[10,11] and it could have broad application to a number of technologically important problems, including the catalytic reactivity of subsurface oxygen and carbon in connection with corrosion, oxidation, or carbonylation processes,[12,13] subsurface hydrogen reactivity for hydrogenation and hydrogenolysis reactions,[14–19] hydrogen storage in and embrittlement of metals,[11,20,21] and the purification of hydrogen fuel streams with Pd-alloy membranes.[22,23]

Here we analyze the effect of strain on the creation of subsurface species in metals by focusing on the hydrogen/nickel system and using periodic, self-consistent density functional theory (DFT) calculations. As recent atomically resolved STM images of surface defects on Ru(0001) showed regions with lattice stretching of up to 10% in the immediate vicinity of these defects,[8] we focused our studies on Ni(111) slabs with 3 and 10% expansive strain. We show that, while very high H_2 pressures are required to produce subsurface hydrogen on perfect, unstretched Ni(111) surfaces,[24] only modest pressures (on the order of tens of bar) are required for subsurface hydrogen to form on the stretched Ni surfaces that might exist in the vicinity of defects. We also demonstrate that strain qualitatively changes both the site preferences of subsurface hydrogen and the character of the stable surface and subsurface phases of the H/Ni(111) system. We discuss these results in the context of defect-mediated penetration of hydrogen into subsurface regions of both single-crystal and polycrystalline nickel catalysts, and we comment on the implications of the results for other processes involving various subsurface species in transition metals.

A summary of the low-coverage ($\theta = 0.25$ ML (ML = monolayer), corresponding to one H atom per four surface Ni atoms) data for the lowest energy sites of surface, first-layer subsurface, and second-layer subsurface hydrogen at three strain levels is given in Table 1. A modest strain effect on the binding energy (BE_H) of surface hydrogen is found (an increase of 0.05 eV in the magnitude of BE_H is calculated between the unstretched and the 10%-stretched slabs), consistent with a calculated upshift of 0.24 eV in the nickel d-band center (see Ruban et al.[3] for a discussion of the relationship between this electronic structure parameter and the surface reactivity). This effect becomes more pronounced for hydrogen in the first and second subsurface layers (strain-related stabilizations of 0.14 and 0.32 eV are calculated in these cases), and this suggests that, at low hydrogen coverages, stretched slabs appear to stabilize subsurface H to a greater extent than surface H.

Table 1: Binding energies BE_H for surface and subsurface hydrogen on slabs with 0, 3, and 10% expansive lattice strain.[a]

Layer	Strain [%]	H site[b]	BE_H [eV][c]
Surface	0	fcc[d]	−2.89[e]
Surface	3	fcc[d]	−2.91[e]
Surface	10	fcc[d]	−2.94[e]
1st subsurface	0	octa	−2.18[e]
1st subsurface	3	octa	−2.28[e]
1st subsurface	10	tetra (under top)	−2.32[e]
2nd subsurface	0	octa	−2.11[f]
2nd subsurface	3	octa	−2.24[f]
2nd subsurface	10	tetra (under top)[d]	−2.43[f]

[a] Total coverage of 0.25 ML on a 2×2 surface unit cell. [b] octa = octahedral, tetra = tetrahedral. [c] The reference state for the hydrogen binding energies is gas-phase atomic H and a clean nickel slab at infinite separation. [d] One or more other sites have energies comparable to the energies of the indicated sites. [e] Four-layer Ni(111) slabs with the top two layers relaxed. [f] Five-layer Ni(111) slabs with the top three layers relaxed.

One-dimensional potential energy surfaces (PESs) for hydrogen diffusion from the surface to the first and second subsurface nickel layers at various strain levels are given in Figure 1. As the Ni(111) surface is stretched from 0 to 3%, the energy at all points along the PES is lowered, and the barriers E^* for hydrogen diffusion from the surface to the first subsurface layer and from the first to the second subsurface

[*] J. Greeley, W. P. Krekelberg, Prof. M. Mavrikakis
Department of Chemical and Biological Engineering
University of Wisconsin-Madison
1415 Engineering Drive, Madison, WI 53706 (USA)
Fax: (+1) 608-262-5434
E-mail: manos@engr.wisc.edu

[**] J.G. acknowledges partial financial support from an NSF predoctoral fellowship. This work was supported through an NSF-CAREER Award (CTS-0134561) and a DOE-BES Catalysis Science Grant (DE-FG02-03ER15469). We thank DOE-NERSC and NSF-NPACI for supercomputing time. Fruitful discussions on the atomic-scale aspects of defects on metal surfaces with Professor Joost Wintterlin are gratefully acknowledged.

  DOI: 10.1002/ange.200454062

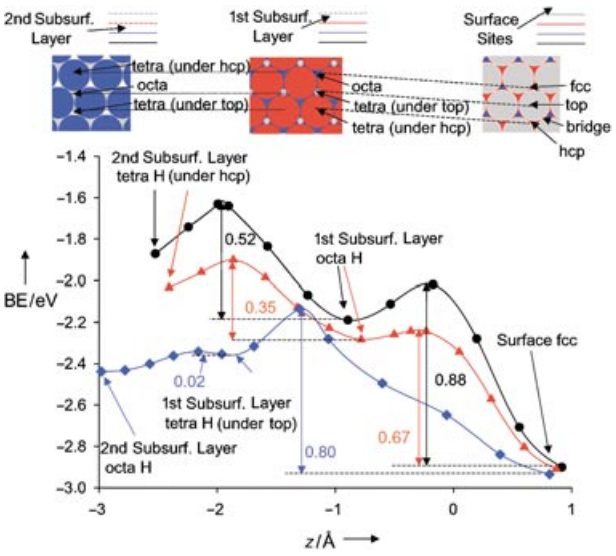

Figure 1. One-dimensional potential energy surface for the sequential diffusion of atomic hydrogen from the surface to the first and second subsurface layers in Ni(111). θ_{total} = 0.25 ML. Diffusion coordinates on slabs with 0, 3, and 10% lattice strain are denoted by black circles, red triangles, and blue diamonds, respectively. z = 0 signifies the position of the first layer of nickel atoms on the respective clean, relaxed nickel slabs, and the z coordinate denotes the distance of the hydrogen atom from this reference point. For diffusion from the surface to the first subsurface layer, four-layer slabs (top two layers relaxed) were used. For diffusion from the first subsurface to the second subsurface layer, five-layer slabs (top three layers relaxed) were used. Data for four-layer slabs are given at the intersection of these regions. Tetra = tetrahedral, octa = octahedral. Insets describe the various surface and subsurface sites; the color of the Ni atoms indicates their location (gray = surface layer, red = first subsurface layer, blue = second subsurface layer). Numerical values represent E* [eV] values.

layer decrease from 0.88 and 0.52 eV to 0.67 and 0.35 eV, respectively. At the same time, the resurfacing barrier for subsurface H (corresponding to movement of hydrogen atoms from subsurface octahedral sites—the lowest energy sites at these strain levels—to surface fcc sites) decreases from 0.17 to 0.04 eV. As the surface is stretched still further, the resurfacing barrier drops to zero, and the octahedral sites become unstable. Thus, for Ni(111) slabs with 10% strain, hydrogen must diffuse to an under-top tetrahedral site to find a stable subsurface configuration. This additional diffusional requirement raises the surface-to-subsurface diffusion barrier to 0.80 eV; this value is greater than the corresponding barrier for 3%-stretched slabs, in which subsurface octahedral sites are still stable, but it is less than the corresponding value for the unstretched surface (0.88 eV). Hydrogen diffusion deeper into the 10%-stretched slab is facile; a barrier of only 0.02 eV exists between the first and second subsurface nickel layers. These kinetic results, in combination with the thermochemical comparison of the 0%- and 10%-stretched slabs described above, suggest that both the thermochemistry and the kinetics of subsurface hydrogen formation are enhanced by expansive strain, which might be present in the vicinity of surface defects.

Thermochemical data for hydrogen coverages up to 2.0 ML at various strain levels are given in Table 2 and Figure 2. For total coverages of 1.0 ML or less and for each strain, the average BE_H value per H atom remains practically constant (only surface sites are occupied at these coverages); the variations in the differential BE_H values are slightly larger. As subsurface sites become populated at higher coverages, and for all strain levels, the magnitude of the average BE_H level per hydrogen atom decreases steadily. At the same time, the magnitude of the differential BE_H value drops quickly (by 0.5–0.7 eV, characterizing the onset of subsurface site occupation) and then increases again (by 0.05–0.10 eV); the increase in the magnitude of the differential BE_H value at higher subsurface coverages may be due to substrate-mediated attraction between the subsurface H atoms. Although these general trends exist for all strain levels examined, certain features of the coverage dependence of the BE_H value are strain-dependent. For example, between 0 and 10% strain, the strength of hydrogen binding increases for all coverages. Interestingly, however, the magnitude of the increase is greater at higher coverages (both the average and

Table 2: Binding energies BE_H per hydrogen atom for low- and high-coverage surface and subsurface hydrogen on and in Ni(111) slabs with 0, 3, and 10% lattice stretching.[a]

Strain [%]	Total hydrogen coverage [ML]	Hydrogen surface and subsurface sites[b]	Average BE_H per hydrogen atom [eV][c]	Differential BE_H [eV][d]
0	0.25	fcc(1)	−2.89	−2.89
0	0.50	fcc(1) + hcp(1)	−2.91	−2.93
0	0.75	fcc(3)	−2.86	−2.77
0	1.00	fcc(4)	−2.86	−2.86
0	1.25	hcp(4) + octa(1)	−2.73	−2.20
0	1.50	hcp(4) + octa(2)	−2.65	−2.26
0	1.75	hcp(4) + octa(3)	−2.60	−2.28
0	2.00	hcp(4) + octa(4)	−2.56	−2.29
3	0.25	fcc(1)	−2.91	−2.91
3	0.50	fcc(2)	−2.90	−2.95
3	0.75	fcc(3)	−2.90	−2.85
3	1.00	fcc(4)	−2.91	−2.93
3	1.25	hcp(4) + octa(1)	−2.78	−2.27
3	1.50	hcp(4) + octa(2)	−2.71	−2.34
3	1.75	hcp(4) + octa(3)	−2.66	−2.36
3	2.00	hcp(4) + octa(4)	−2.62	−2.38
10	0.25	fcc(1)	−2.94	−2.94
10	0.50	fcc(2)	−2.95	−2.96
10	0.75	fcc(3)	−2.96	−2.98
10	1.00	fcc(4)	−2.97	−3.02
10	1.25	fcc(4) + tetra(1)	−2.87	−2.44
10	1.50	fcc(4) + tetra(2)	−2.80	−2.46
10	1.75	fcc(4) + tetra(3)	−2.75	−2.48
10	2.00	fcc(4) + tetra(4)	−2.72	−2.50

[a] All calculations were performed on 2×2×4 slabs with the top two layers relaxed. [b] octa = octahedral, tetra = tetrahedral under top (directly under a Ni atom). The numbers in parenthesis indicate how many of these sites are populated in the specific configuration. Only the lowest energy configurations calculated at each coverage are shown. [c] The reference state for the BE_H is gas-phase atomic H and a clean nickel slab at infinite separation. [d] The differential binding energy is the energy change for the reaction $H(g) + nH/Ni(111) \rightarrow (n+1)H/Ni(111)$.

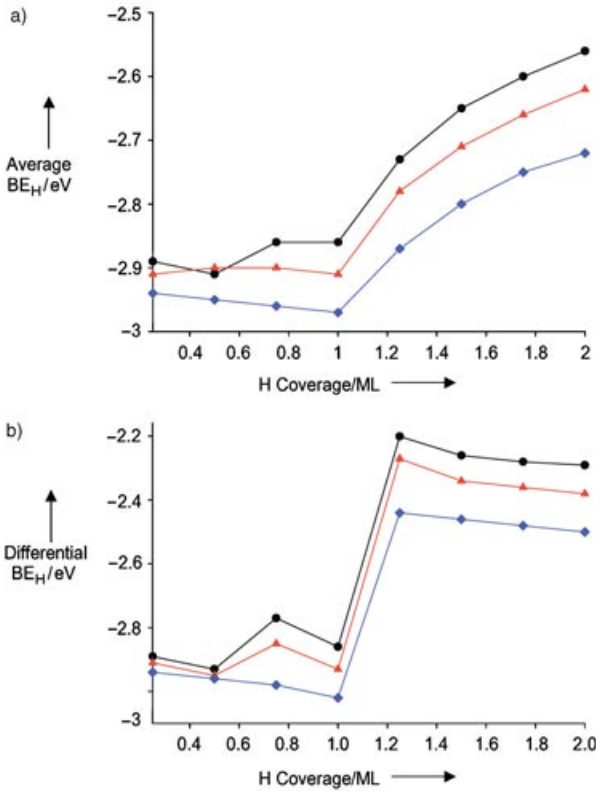

Figure 2. a) Average BE_H as a function of total hydrogen coverage. Black circles, red triangles, and blue diamonds denote BE_H on slabs with 0, 3, and 10% strain, respectively. b) Differential BE_H (defined in Table 2) as a function of total hydrogen coverage .

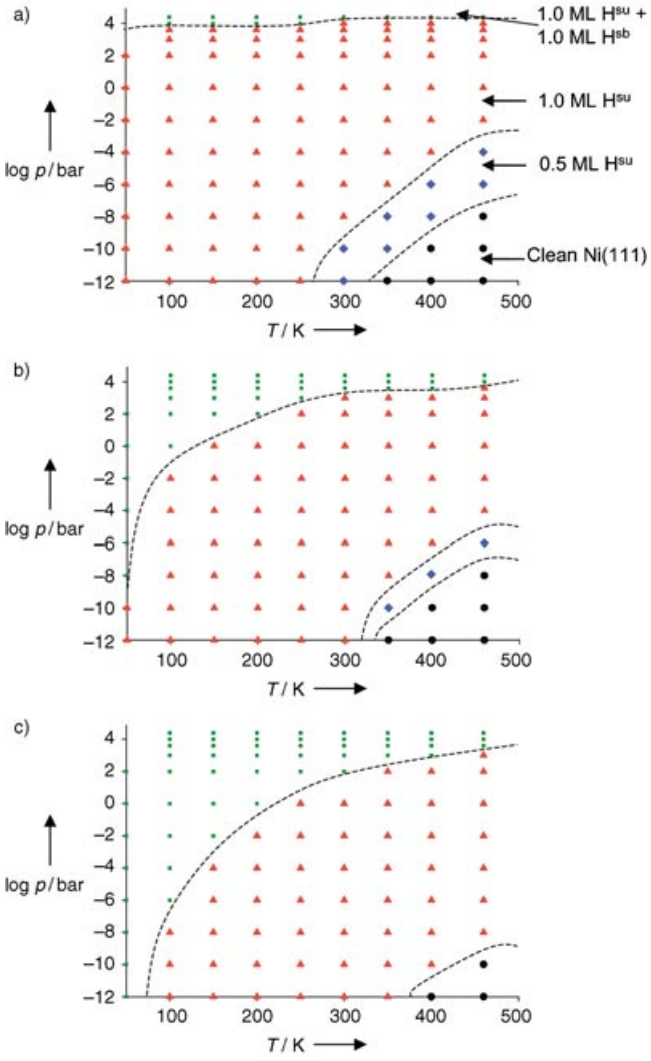

Figure 3. Phase diagrams for surface and subsurface hydrogen on Ni(111) slabs at a) 0, b) 3, and c) 10% lattice strain. See Table 2 for details of the corresponding configurations. Zero-point energy corrections are included for all coverages. The lines between different phases represent, in an approximate manner, the corresponding phase transitions. H^{su} = surface hydrogen, H^{sb} = subsurface hydrogen.

differential BE_H magnitudes increase by 0.05 eV between 0 and 10% strain at $\theta = 0.25$ ML, while the corresponding increases at a total coverage of 2.0 ML are 0.16 and 0.21 eV, respectively). This result demonstrates that the greater expansive-strain-induced stabilization of subsurface H over surface H, described above for hydrogen coverages of 0.25 ML, is even more pronounced at higher coverages. Thus, we suggest that expansive strain may facilitate the thermochemistry of subsurface species formation more dramatically at higher coverages than at lower coverages.

Phase diagrams for H on/in Ni(111) surfaces with 0, 3, and 10% strain (including approximate zero-point energy corrections) are given in Figure 3. The diagrams are constructed under the assumption that an effective equilibrium condition exists between the surface region (represented by our Ni(111) slabs with ad(b)sorbed hydrogen; see Theoretical Section) and both a gas-phase H_2 reservior and a bulk nickel reservoir. We note that a suitable nickel reservoir will be present provided that hydrogen is confined in a local energy minimum near the surface (this will be the case if the timescale for hydrogen transfer from the gas phase to the surface region is much shorter than that for hydrogen population of the bulk nickel reservoir; see Christensen et al.[25] for analogous discussions).[24,26,27] Although no experimental data are available with which to compare the stretched-slab results, the phase diagram on the unstretched slab has been shown to give good agreement with experiment.[24,28,29] The broad trends in each of the phase diagrams are similar; increasing pressure and decreasing temperature favor higher total coverages of hydrogen. Also, we note that, in each diagram, the phases that are present correspond to the minima in the differential BE_H values versus coverage graph (Figure 2b; the minima in the graph indicate stronger binding). However, the relative sizes of the various coverage regimes on the phase diagrams change significantly as a function of strain. As the surface is stretched, the 1.0 ML H phase (surface hydrogen only) and the clean surface phase become smaller, while the 0.5 ML H phase (surface only) is completely absent for the 10%-stretched slab. In contrast, as the surface is stretched, the 2.0 ML phase, where 1.0 ML of subsurface H is present, increases substantially in size. In consequence, whereas pressures on the order of thousands of bar are required to produce subsurface hydrogen from H_2(g) at room temperature on an unstretched Ni(111) surface, pressures of only

tens of bar are required for production of subsurface H on slabs with 10% strain.

The above results demonstrate that subsurface hydrogen will form more readily in stretched regions of Ni surfaces than in unstretched regions. The kinetics of subsurface H formation are improved, as evidenced by the lower barrier for surface-to-subsurface diffusion on stretched surfaces, and this suggests that population of subsurface sites will occur more rapidly in stretched regions. For example, if differences in preexponential factors are neglected, the 0.21 eV difference in diffusion barriers between surface and first subsurface layers (Figure 1) suggests that the rate constant for hydrogen penetration to the first subsurface layer will be about 3500 times higher on 3%-stretched than on unstretched slabs at room temperature. Further, and more significantly, subsurface hydrogen will be thermodynamically stable at much lower pressures and/or at higher temperatures in stretched areas than in unstretched regions. This information, when combined with insights from recent work showing that large stretched areas are induced in crystal surfaces by dislocations that originate in the bulk,[8] implies that nickel crystals with such defects will absorb hydrogen more readily than perfect Ni(111) surfaces. This mechanism for strain-mediated formation of subsurface hydrogen around defects, possibly combined with previous proposals for subsurface H formation by grain-boundary diffusion and/or direct hydrogen penetration through steps and kinks,[11,30] could explain the observed higher solubility of hydrogen in polycrystalline, as opposed to single-crystal, nickel samples.[31] In turn, we suggest that, if subsurface species play a special role in catalytic surface chemistry, that role might be more pronounced on real catalytic particles, where defect density is much higher than on single crystal surfaces. We note that, for extremely small catalytic nanoparticles, bulk-induced defects will be less common, and compressive strain (a general characteristic of such small nanoparticles),[32,33] as opposed to the stretching described above, may dominate the characteristics of the particle. Thus, the changes in absorptive and catalytic properties of nickel described here will not apply to the very smallest nickel nanoparticles.

The relationship between strain and formation of subsurface species, described above for the particular case of subsurface hydrogen in nickel, may have important implications for other systems in which subsurface heteroatoms play a significant role. Corrosion, embrittlement, hydrogenation, hydrogen storage, and hydrogen purification processes may all be influenced by such effects. As such, in addition to providing insights into the differences between these processes on single-crystal and polycrystalline metals, a careful study of the effect of strain on these systems could provide novel, as-yet unanticipated, insights into the basic chemical and physical processes that underlie them.

Theoretical Section

To study the effect of strain on formation of subsurface hydrogen, we used DFT calculations. Many of the details of both the DFT calculations and the construction of the phase diagrams have been described previously,[24] and here we give only a brief summary. DACAPO, the periodic, self-consistent, DFT-based total energy code, was used for all calculations.[34,35] The GGA-PW91 functional was employed,[36,37] and four- or five-layer slabs (with the top two or three layers relaxed, respectively) with a 2×2 surface unit cell were used. Zero-point energies were included in the results only where explicitly specified. Both gas-phase atomic H and Ni(111) slabs (clean and hydrogen-covered) were treated with fully spin-polarized calculations. To simulate stretched nickel surfaces, the lattice constant d of the unit cell was increased from the unstretched value of 3.52 Å to 3.62 Å and then to 3.87 Å, corresponding to relative strain values $\Delta d/d_{eq}$ of about 3 and 10%, respectively, a range suggested by recent atomically resolved STM measurements on single-crystal transition metal surfaces.[8] For all calculations on stretched slabs, the Ni–Ni interlayer distance was kept at its unstretched value (although the top two or three layers were still allowed to relax according to the Hellman–Feynman forces) to simulate strain in directions parallel to the surface only. Phase diagrams for surface and subsurface hydrogen were constructed by determining the state with the lowest grand canonical potential (we note that the periodic boundary conditions employed in the calculations prevent the analysis of disordered phases); the temperature and pressure behavior was calculated by assuming chemical equilibrium between hydrogen on the surface and in the gas phase.

Received: February 20, 2004 [Z54062]

Keywords: density functional calculations · hydrogen · phase diagrams · strain effects · surface chemistry

[1] M. Gsell, P. Jakob, D. Menzel, *Science* **1998**, *280*, 717.
[2] A. Schlapka, M. Lischka, A. Groß, U. Käsberger, P. Jakob, *Phys. Rev. Lett.* **2003**, *91*, 016101.
[3] A. Ruban, B. Hammer, P. Stoltze, H. L. Skriver, J. K. Nørskov, *J. Mol. Catal. A* **1997**, *115*, 421.
[4] M. Mavrikakis, B. Hammer, J. K. Nørskov, *Phys. Rev. Lett.* **1998**, *81*, 2819.
[5] E. Kampshoff, E. Hahn, K. Kern, *Phys. Rev. Lett.* **1994**, *73*, 704.
[6] J. A. Rodriguez, D. W. Goodman, *Science* **1992**, *257*, 897.
[7] M. K. Rose, A. Borg, T. Mitsui, D. F. Ogletree, M. Salmeron, *J. Chem. Phys.* **2001**, *115*, 10927.
[8] J. Wintterlin, T. Zambelli, J. Trost, J. Greeley, M. Mavrikakis, *Angew. Chem.* **2003**, *115*, 2956; *Angew. Chem. Int. Ed.* **2003**, *42*, 2850.
[9] S. Dahl, A. Logadottir, R. C. Egeberg, J. H. Larsen, I. Chorkendorff, E. Törnqvist, J. K. Nørskov, *Phys. Rev. Lett.* **1999**, *83*, 1814.
[10] A. D. Johnson, K. J. Maynard, S. P. Daley, Q. Y. Yang, S. T. Ceyer, *Phys. Rev. Lett.* **1991**, *67*, 927.
[11] *Hydrogen in Metals II*, *Vol. 29* (Eds.: G. Alefeld, J. Völkl), Springer, Berlin, **1978**.
[12] A. Knop-Gericke, M. Hävecker, T. Schedel-Niedrig, R. Schlögl, *Top. Catal.* **2001**, *15*, 27.
[13] M. P. Ryan, D. E. Williams, R. J. Chater, B. M. Hutton, D. S. McPhail, *Nature* **2002**, *415*, 770.
[14] A. D. Johnson, S. P. Daley, A. L. Utz, S. T. Ceyer, *Science* **1992**, *257*, 223.
[15] S. T. Ceyer, *Acc. Chem. Res.* **2001**, *34*, 737.
[16] X. Sha, B. Jackson, *Chem. Phys. Lett.* **2002**, *357*, 389.
[17] A. Michaelides, P. Hu, A. Alavi, *J. Chem. Phys.* **1999**, *111*, 1343.
[18] V. Ledentu, W. Dong, P. Sautet, *J. Am. Chem. Soc.* **2000**, *122*, 1796.
[19] G. Henkelman, A. Arnaldsson, H. Jónsson, *Surf. Sci.*, submitted.
[20] W. Zhong, Y. Cai, D. Tomanek, *Nature* **1993**, *362*, 435.
[21] C. Elsässer, H. Krimmel, M. Fähnle, S. G. Louie, C. T. Chan, *J. Phys. Condens. Matter* **1998**, *10*, 5131.
[22] K. Hou, R. Hughes, *J. Membr. Sci.* **2003**, *214*, 43.
[23] D. R. Alfonso, A. V. Cugini, D. S. Sholl, *Surf. Sci.* **2003**, *546*, 12.

[24] J. Greeley, M. Mavrikakis, *Surf. Sci.* **2003**, *540*, 215.
[25] A. Christensen, A. V. Ruban, P. Stoltze, K. W. Jacobsen, H. L. Skriver, J. K. Nørskov, F. Besenbacher, *Phys. Rev. B* **1997**, *56*, 5822.
[26] M. V. Bollinger, K. W. Jacobsen, J. K. Nørskov, *Phys. Rev. B* **2003**, *67*, 085410.
[27] N. Moll, A. Kley, E. Pehlke, M. Scheffler, *Phys. Rev. B* **1996**, *54*, 8844.
[28] K. Christmann, O. Schober, G. Ertl, M. Neumann, *J. Chem. Phys.* **1974**, *60*, 4528.
[29] K. Christmann, R. J. Behm, G. Ertl, M. A. Van Hove, W. H. Weinberg, *J. Chem. Phys.* **1979**, *70*, 4168.
[30] K. Haug, G. Raibeck, *J. Phys. Chem. B* **2003**, *107*, 11433.
[31] S. W. Stafford, R. B. McLellan, *Acta Metall.* **1974**, *22*, 1463.
[32] P. Nava, M. Sierka, R. Ahlrichs, *Phys. Chem. Chem. Phys.* **2003**, *5*, 3372.
[33] M. Klimenkov, S. Nepijko, H. Kuhlenbeck, M. Bäumer, R. Schlögl, H.-J. Freund, *Surf. Sci.* **1997**, *391*, 27.
[34] B. Hammer, L. B. Hansen, J. K. Nørskov, *Phys. Rev. B* **1999**, *59*, 7413.
[35] J. Greeley, J. K. Nørskov, M. Mavrikakis, *Annu. Rev. Phys. Chem.* **2002**, *53*, 319.
[36] J. P. Perdew, J. A. Chevary, S. H. Vosko, K. A. Jackson, M. R. Pederson, D. J. Singh, C. Fiolhais, *Phys. Rev. B* **1992**, *46*, 6671.
[37] J. A. White, D. M. Bird, *Phys. Rev. B* **1994**, *50*, 4954.

